British Journal of Cancer

ARTICLE

Check for updates

Cellular and Molecular Biology

Periostin–TGF-β feedforward loop contributes to tumour-stroma crosstalk in liver metastatic outgrowth of colorectal cancer

Bin Liu[1,2,5], Tiantian Wu[1,2,5], Biyu Lin[1,5], Xingxing Liu[1,2], Yingfu Liu[2,3], Gang Song[3]✉, Chuannan Fan[1,4]✉ and Gaoliang Ouyang[1,2]✉

BACKGROUND: This study aimed to investigate the underlying mechanisms of matricellular protein periostin (POSTN) on tumour-stroma crosstalk in the liver metastatic microenvironment of colorectal cancer (CRC).

METHODS: *Postn*-knockout mice and hepatic *Postn*-overexpressing mice were used to investigate the functions of POSTN on the formation of fibrotic microenvironment and the tumour-stroma crosstalk in the liver metastatic microenvironment of CRC. Clinical samples and database were analyzed to show the correlation between POSTN expression and fibrotic features and TGF-β signalling in metastatic livers of CRC.

RESULTS: POSTN deficiency reduced hepatic stellate cell (HSC) activation and liver metastasis, whereas POSTN overexpression in the liver significantly augmented the formation of a fibrotic microenvironment to support the liver metastatic growth of CRC cells in mice. Moreover, HSC-derived POSTN promoted TGF-β1 expression in CRC cells through the integrin/FAK/ERK/STAT3 pathway; conversely, tumour cell-derived TGF-β1 induced POSTN expression in HSCs via the Smad pathway. POSTN levels correlated with fibrotic features and TGF-β signalling in metastatic liver tissues of CRC patients.

CONCLUSIONS: POSTN and TGF-β1 cooperatively contribute to the tumour-stroma crosstalk by forming a supporting fibrotic microenvironment to promote liver metastasis of CRC cells via the POSTN/integrin/FAK/ERK/STAT3/TGF-β axis in tumour cells and TGF-β/Smad/POSTN signalling in activated HSCs.

British Journal of Cancer (2024) 130:358–368; https://doi.org/10.1038/s41416-023-02516-3

INTRODUCTION

Colorectal cancer (CRC) is one of the most common malignant neoplasms worldwide [1]. CRC originates from benign lesions of adenomatous polyps in the intestine and eventually develops into highly invasive carcinoma. Once colorectal tumour cells invade the underlying colorectal wall, more than 80% of CRC patients would rapidly develop liver metastases, which are the major cause of death in CRC patients [2–4]. Recent studies have demonstrated that interactions between tumour cells and stromal cells in the metastatic liver govern their fate and subsequent metastatic colonization in the livers [5–7]. As a major component of the tumour microenvironment, the extracellular matrix (ECM) modulates the dissemination, adhesion, survival, and growth of cancer cells in metastatic organs [8, 9]. However, the underlying mechanisms of ECM components on tumour-stroma interaction in liver metastasis of CRC cells remain largely unknown.

Periostin (POSTN) is a secreted component of the ECM and is considered a critical mediator of tissue remodeling and fibrosis in various organs [10–13]. Current evidence also demonstrates that POSTN plays an important role in tumourigenesis and metastasis [14–17]. Recently, we demonstrated that fibroblast-derived POSTN induces IL-6 secretion in colorectal tumour cells whereas tumour cell-derived IL-6 increases POSTN expression in fibroblasts; thus, fibroblast-derived POSTN and tumour cell-secreted IL-6 work cooperatively to promote tumourigenesis in AOM/DSS-treated mice and in *APC*$^{min/+}$ mice [18]. We also found that POSTN deficiency reduces the infiltration of PD-1^{+} tumour-associated macrophages (TAMs) and enhances the phagocytosis of TAMs, thus decreasing the immune evasion of tumour cells in CRC [19]. Moreover, ectopic overexpression of POSTN in colorectal tumour cells promotes metastatic growth of CRC cells in the liver [20]. However, it is still largely unclear how POSTN serves as a link between tumour cells and stromal cells in the metastatic liver of CRC.

Here, we found that POSTN deficiency alleviates the formation of a fibrotic microenvironment in the metastatic liver and inhibits

[1]State Key Laboratory of Cellular Stress Biology, School of Life Sciences, Faculty of Medicine and Life Sciences, Xiamen University, Xiamen, China. [2]Department of Hematology, the First Affiliated Hospital of Xiamen University and Institute of Hematology, School of Medicine, Xiamen University, Xiamen, China. [3]Department of Basic Medical Sciences, School of Medicine, Xiamen University, Xiamen, China. [4]Department of Cell and Chemical Biology and Oncode Institute, Leiden University Medical Center, Leiden, The Netherlands. [5]These authors contributed equally: Bin Liu, Tiantian Wu, Biyu Lin. ✉email: gangsongsd@xmu.edu.cn; C.Fan@lumc.nl; oygldz@xmu.edu.cn

Received: 24 February 2023 Revised: 16 November 2023 Accepted: 22 November 2023
Published online: 14 December 2023

the metastatic outgrowth of CRC cells in mice, whereas overexpression of POSTN in the liver significantly augments the formation of a fibrotic microenvironment to support the metastatic growth of CRC cells in the livers of mice. Moreover, hepatic stellate cell (HSC)-derived POSTN promotes the expression of TGF-β1 in CRC cells by activating the integrin/FAK/ERK/STAT3 pathway, whereas tumour cell-derived TGF-β1 increases the expression of POSTN in HSCs via the Smad pathway. Our data demonstrate that POSTN and TGF-β1 cooperatively contribute to the tumour-stroma crosstalk by forming a supporting fibrotic microenvironment to promote liver metastasis of CRC cells via the POSTN/integrin/FAK/ERK/STAT3/TGF-β axis in tumour cells and TGF-β/Smad/POSTN signalling in activated HSCs.

MATERIALS AND METHODS

Animal experiments

Postn$^{+/-}$ mice with a C57BL/6 background were purchased from the Jackson Laboratory. Wild-type and POSTN-deficient C57BL/6 mice were generated by crossing *Postn*$^{+/-}$ mice with *Postn*$^{+/-}$ mice as previously described [17]. Wild-type and POSTN-deficient mice with a Balb/c background were generated, similar to the C57BL/6 background mice.

A liver metastasis model was constructed in 6-to-8-week-old wild-type and POSTN-deficient male mice by intrasplenic injection of 5×10^5 CRC cells and the bioluminescent signals in mice were examined three weeks after injection using a live animal Lumina II system (Xenogen IVIS System). Overexpression of POSTN or GFP in the livers of mice was achieved by tail vein injection with adenovirus-*Postn* (Ad-Postn) or adenovirus-GFP (Ad-GFP) (2×10^9 plaque-forming units) 2 days after intraperitoneal injection of CRC cells, and the bioluminescent signals in mice were examined 2 weeks after injection. Recombinant adenoviruses were obtained from Prof. Xiaoying Li (Shanghai Jiao Tong University School of Medicine, Shanghai, China) [21].

All animal experiments were conducted in accordance with animal protocols approved by the Animal Care and Use Committee of Xiamen University.

Liver histology

Liver tissues were fixed overnight in 4% paraformaldehyde and embedded in paraffin, and serial sections were stained with hematoxylin and eosin (H&E), Sirius red, immunohistochemical and immunofluorescence staining.

For immunohistochemical staining, deparaffinization and rehydration steps were carried out on tissue sections, and the antigen was retrieved with 0.01 M sodium citrate buffer. Pre-treated sections were blocked with normal goat serum at room temperature and incubated with primary antibodies (1:200 dilution) overnight at 4 °C. The sections were washed and incubated with streptavidin-horseradish peroxidase-conjugated secondary antibodies for 1 h at room temperature. The signal was detected using DAB staining.

For immunofluorescence staining, liver tissues were embedded in OCT (Sakura) and frozen at −20 °C. Tissue sections were baked at 37 °C for 1.5 h, fixed with ice-cold acetone for 10 min, washed with PBS, and blocked with a blocking solution for 1 h. The tissue sections were incubated with primary antibodies overnight at 4 °C. The sections were washed and incubated with the corresponding secondary antibodies for 1 h in the dark. After washing with PBS, the sections were stained with Hoechst. Stained sections were mounted on slides for immunofluorescence analysis using a fluorescence microscope (Zeiss LSM 780). The antibodies used in this study are listed in the Supplementary Table S1.

Quantitative real-time PCR

Total RNA was extracted from fresh liver tissues or cultured cells using TRIzol reagent (Invitrogen) according to the manufacturer's instructions. Reverse transcription was performed using a ReverTra Ace qPCR RT Kit (Toyobo). The relative levels of various target genes were quantified using the $2^{-\Delta\Delta Ct}$ formula with *GAPDH* RNA as the reference transcript for normalization. The relative mRNA levels were shown as fold-changes over the corresponding control value. The primers used are listed in the Supplementary Table S2.

Cell culture

CRC cell lines and the human hepatic stellate cell line LX-2 were purchased from the ATCC and tested for free from Mycoplasma infection by MycoBlue Mycoplasma Detector (Vazyme). The murine CRC cell lines CT26 and CMT93 and the human CRC cell line SW620 were cultured in Dulbecco's modified DMEM medium (DMEM; Gibco) with 10% foetal bovine serum (HyClone) and 1% penicillin-streptomycin (Gibco). The lentivirus-mediated packaging system was used to generate luciferase-expressing cell lines CMT93-luc and CT26-luc. After high-titre lentiviruses were added to infect the cells, puromycin was added to select cell lines with stable firefly luciferase expression. All the cell lines were maintained at 37°C with 5% CO_2 in a humidified atmosphere.

Co-culture of SW620 cells with LX-2 cells was conducted in serum-free DMEM using 6-well plates with 0.4-μm pore size Transwell chambers (Costar; 3412). LX-2 cells were seeded in 6-well plates at 6×10^5 cells/well and SW620 cells were added to the upper chamber at 2×10^5 cells/well.

Recombinant protein treatment

For recombinant POSTN or TGF-β1 treatment experiment, CMT93, SW620 cells or HSCs were serum-starved for 12 h, and then stimulated with 200 ng/ml recombinant human or mouse POSTN (rhPOSTN or rmPOSTN) (R&D Systems) or 10 ng/ml recombinant human TGF-β1 (R&D Systems).

Western blot analysis

Liver tissues were homogenized in radioimmunoprecipitation (RIPA) lysis buffer supplemented with PhosSTOP™ phosphatase inhibitor (Roche). The samples were centrifuged at 13,000 rpm for 10 min at 4 °C and the soluble supernatants were retained. The total protein concentration was measured using a BCA Protein Assay kit (Thermo Scientific). Proteins were separated by electrophoresis on 6–10% polyacrylamide gels and transferred onto nitrocellulose membranes (Millipore). The membranes were blocked with Tris-buffered saline and 0.1% Tween 20 (TBST) containing 5% bovine serum albumin (BSA), and then incubated with primary antibodies at 4 °C overnight. After washing three times with TBST buffer at room temperature, the membranes were incubated with secondary antibodies for 1 h. The membranes were washed, incubated with ECL Western Blot Substrate (Millipore), and visualized on X-ray films. The antibodies used in this study are listed in the Supplementary Table S1. All the original western blots were included in the "original data file".

Luciferase reporter assay

The luciferase activity was evaluated by using the Dual Luciferase Assay System, as described by the manufacturer (Promega). Transient transfections of the indicated firefly luciferase reporters and Renilla luciferase, which served as a transfection internal control, were performed using polyethylenimine (PEI) reagent. Cells were lysed in 1 × Passive Lysis Buffer, and signals were measured using the Dual Luciferase Reporter Assay System. Firefly luciferase activity was normalized to Renilla luciferase activity, and data were expressed as fold-induction in the experimental condition compared to the control.

Clinical tissue samples

Human clinical samples were collected with informed consent from the patients. The collection and study of human clinical samples were performed in accordance with the approved guidelines of the Ethics and Scientific Committees of Xiamen Hospital of Traditional Chinese Medicine.

Statistical analysis

All results are presented as the mean ± standard error of the mean (SEM). Independent biological replicates were chosen in advance and are indicated in figure legends. Statistical analyses were performed using Student's *t* test for normally distributed data or one-way ANOVA test to evaluate differences among groups when three or more groups were analyzed. $p < 0.05$ was considered statistically significant.

RESULTS

POSTN is highly expressed in the fibrotic metastatic livers of mice

Metastatic tumour cells can induce the formation of a hepatic fibrotic metastatic microenvironment that facilitates metastatic outgrowth in the liver [7]. Our previous work demonstrated that POSTN is highly expressed in metastatic livers of CRC patients [20]; however, it remains unknown whether highly expressed POSTN is involved in the formation of a fibrotic metastatic microenvironment in the liver. Here, we found that collagen deposition and POSTN

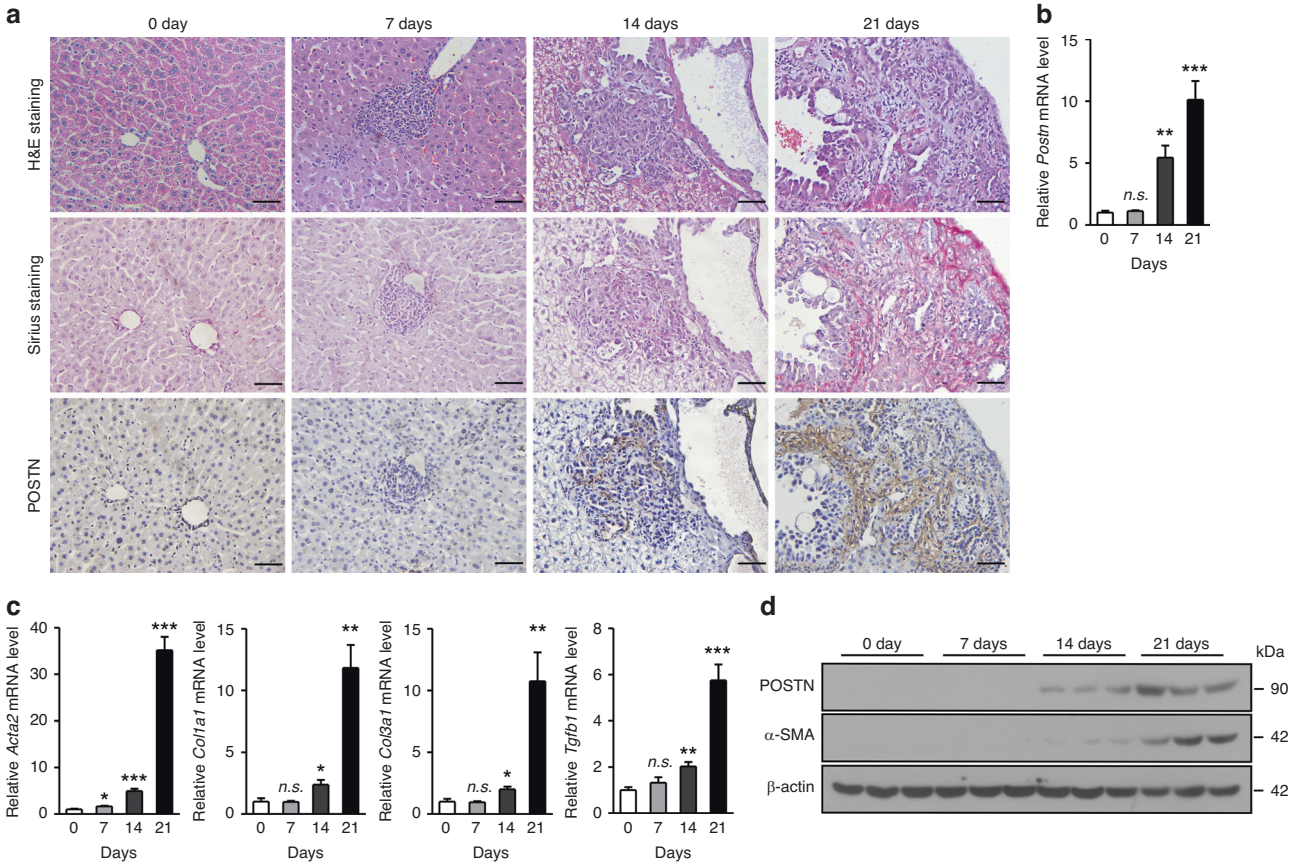

Fig. 1 POSTN is highly expressed in the fibrotic metastatic microenvironment. a H&E staining (upper panels), Sirius Red staining (middle panels) and immunohistochemistry of POSTN (lower panels) in the liver sections of mice 0, 7, 14 and 21 days after intrasplenic injection with CMT93 colorectal tumour cells. Scare bars, 50 μm. qRT-PCR detection for mRNA levels of *Postn* (**b**) and the indicated fibrosis-related genes (*Acta2*, *Col1a1*, *Col3a1* and *Tgfb1*) (**c**) in the livers of mice 0, 7, 14, 21 days after injection. **d** Western blot analysis of POSTN and α-SMA in the livers of mice 0, 7, 14, 21 days after injection. *, $p < 0.05$; **, $p < 0.01$; ***, $p < 0.001$; n.s., not significant.

expression were increased in the metastatic livers of mice intrasplenically injected with murine CRC cell line CMT93 (Fig. 1a). We further analyzed the mRNA levels of *Postn* and fibrotic markers, including *Acta2*, *Col1a1*, *Col3a1*, and *Tgfb1*, at different time points after intrasplenic injection. Compared with normal liver tissues, the mRNA levels of *Postn* and fibrotic markers significantly increased on days 14 and 21 in metastatic liver samples (Fig. 1b, c). Western blot analysis further revealed the upregulation of POSTN and α-SMA in metastatic livers (Fig. 1d). Moreover, POSTN co-localized with α-SMA and collagen I in the stroma, indicating that POSTN is mainly derived from activated HSCs (Supplementary Fig. S1). Our previous studies demonstrated that POSTN is mainly derived from activated HSCs in liver tumours and fibrotic livers, and POSTN can be regarded as a marker of HSC activation, similar to α-SMA, in liver tumours [12, 22]. These results indicate that HSC-derived POSTN is highly expressed in the fibrotic microenvironment of metastatic livers of mice injected with CRC cells.

POSTN deficiency reduces the fibrotic metastatic microenvironment formation and metastatic colonization of CRC cells in mouse livers

After determining that POSTN is highly expressed in the hepatic fibrotic microenvironment in metastatic livers, we further investigated the effect of POSTN deficiency on liver metastasis of CRC cells. We intrasplenically injected CMT93 colorectal tumour cells labelled with luciferase (CMT93-Luc) into wild-type and *Postn*-knockout mice on a C57BL/6 background. Three weeks after implantation, the metastatic lesions were analyzed using live bioluminescence imaging. The size of liver metastases in *Postn*-knockout mice was significantly smaller than that in wild-type mice (Fig. 2a, b and Supplementary Fig. S2A). Moreover, the liver/body weight ratio was significantly lower in *Postn*-knockout mice (Fig. 2c). H&E staining showed that the metastatic areas were dramatically decreased in the livers of *Postn*-knockout mice compared with those of wild-type mice (Fig. 2d). Additionally, fewer Ki67-positive cells were observed in *Postn*-knockout mice, indicating that the metastatic outgrowth of CRC cells in the liver is alleviated in the *Postn*-deficient microenvironment (Fig. 2e). Furthermore, Sirius Red staining showed that fewer collagens were deposited in the metastatic livers of *Postn*-knockout mice (Fig. 2f). Quantitative gene expression analysis of HSC activation markers, such as *Acta2*, *Col1a1*, *Col3a1*, and *Tgfb1*, further confirmed that POSTN deficiency significantly decreased HSC activation in the liver (Fig. 2g). We then analyzed α-SMA protein levels by western blotting and found that α-SMA expression was greatly reduced in the liver extracts from *Postn*-knockout mice (Fig. 2h). In line with this result, immunofluorescence analysis revealed that both α-SMA and collagen I were downregulated in the livers of *Postn*-knockout mice (Fig. 2i).

To further confirm the effect of POSTN deficiency on liver metastasis of CRC cells, we intrasplenically injected the murine CRC cell line CT26, which was labelled with luciferase (CT26-Luc), into BALB/c mice. We also found that *Postn*-knockout mice showed decreased metastatic burden, fewer Ki67-positive cells, and lower levels of fibrotic markers than wild-type mice (Fig. 3a–i

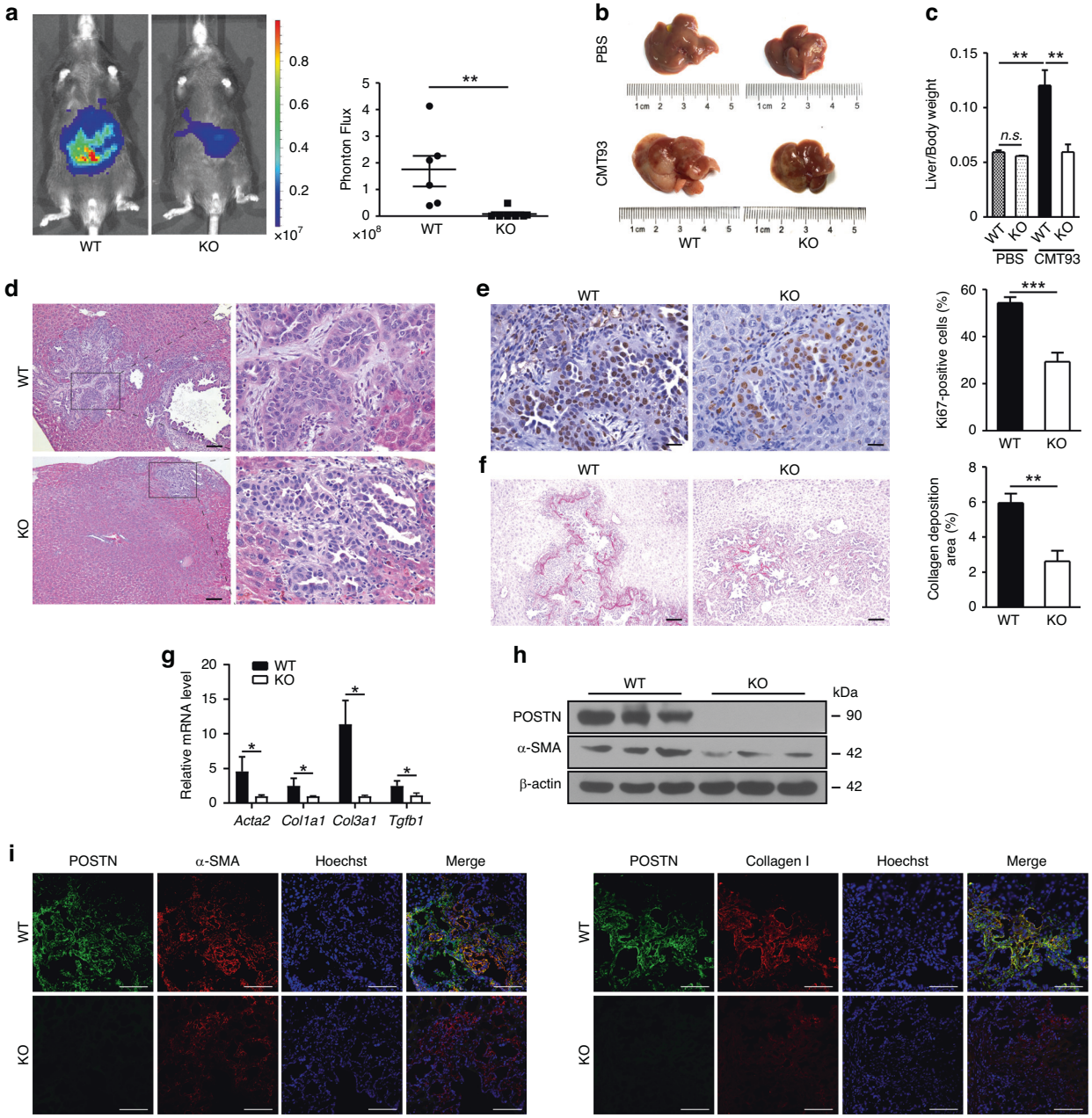

Fig. 2 POSTN deficiency reduces the fibrotic metastatic microenvironment formation and metastatic colonization of CMT93 colorectal tumour cells in the livers of C57BL/6 mice. a Bioluminescent imaging and quantification of metastatic lesions in wild-type (WT) ($n = 6$) or *Postn*-knockout (KO) mice ($n = 7$) 21 days after intrasplenic injection of CMT93-Luc cells. **b**, **c** Representative liver images (**b**) and liver:body weight ratio (**c**) of WT or KO mice in the group presented in (**a**). **d** H&E staining of metastatic liver sections of mice 21 days after cell injection. Scare bars, 100 μm. **e** Representative immunohistochemical staining images and quantification of Ki67-positive tumour cells in metastatic livers of mice. Scare bars, 50 μm. **f** Sirius Red staining and quantification of collagen deposition. Scare bars, 100 μm. **g** qRT-PCR measurement for mRNA levels of the indicated fibrotic genes. Western blot analysis of POSTN and α-SMA (**h**) and immunofluorescent co-staining for POSTN and α-SMA/collagen I (**i**) in metastatic livers. Scare bars, 100 μm. *, $p < 0.05$; **, $p < 0.01$; ***, $p < 0.001$; n.s., not significant.

and Supplementary Fig. S2B). Taken together, these findings demonstrate that POSTN deficiency attenuates the formation of a fibrotic microenvironment and inhibits the metastatic growth of CRC cells in the livers of mice.

POSTN overexpression promotes the fibrotic metastatic microenvironment formation and metastatic colonization of CRC cells in mouse livers

To further investigate the function of POSTN in the development of liver metastasis, we overexpressed POSTN in the liver by delivering an adenoviral vector with *Postn* (Ad-Postn) via tail vein injection two days after intrasplenic injection of CMT93-Luc cells. Two weeks later, we observed that the mice injected with Ad-Postn had larger liver metastatic nodules than those injected with Ad-GFP (Fig. 4a, b and Supplementary Fig. S2C). Moreover, the liver/body weight ratio significantly increased in the Ad-Postn injection group (Fig. 4c). Compared to the control group, Ad-Postn-injected mice showed increased metastatic colonization (Fig. 4d) and more Ki67-positive cells in the metastatic areas (Fig. 4e). Furthermore, the deposition of collagens (Fig. 4f) and the mRNA (Fig. 4g) and protein (Fig. 4h)

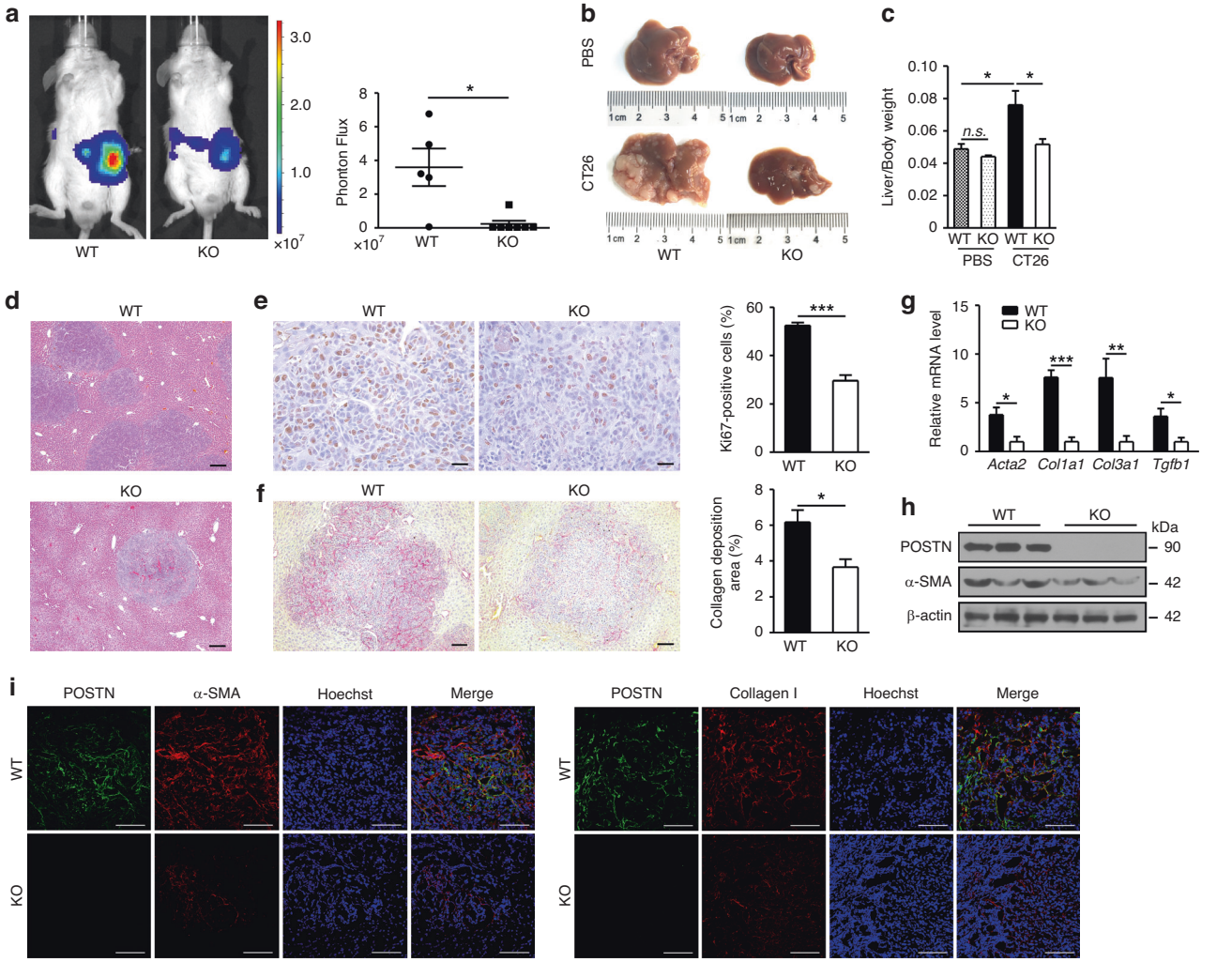

Fig. 3 POSTN deficiency reduces the fibrotic metastatic microenvironment formation and metastatic colonization of CT26 colorectal tumour cells in the livers of BALB/C mice. a Bioluminescent imaging and quantification of metastatic lesions of WT ($n = 5$) or KO mice ($n = 7$) at 21 days after the intrasplenic implantation of CT26-Luc cells. **b**, **c** Representative liver images (**b**) and liver:body weight ratio (**c**) of WT or KO mice in groups presented in (**a**). **d** H&E staining of metastatic liver sections of mice 21 days after cell injection. Scare bars, 100 μm. **e** Representative immunohistochemical staining images and the quantification of Ki67-positive tumour cells in metastatic livers of mice. Scare bars, 50 μm. **f** Sirius Red staining and quantification of collagen deposition. Scare bars, 100 μm. **g** qRT-PCR for mRNA levels of the indicated fibrotic genes. Western blot analysis of POSTN and α-SMA (**h**) and immunofluorescent co-staining for POSTN and α-SMA/collagen I (**i**) in metastatic livers. Scare bars, 100 μm. *, $p < 0.05$; **, $p < 0.01$; ***, $p < 0.001$; n.s., not significant.

levels of fibrosis-associated markers were also specifically increased in the metastatic livers of Ad-Postn mice. Immunofluorescent staining showed that POSTN overexpression increased the levels of α-SMA and collagen I in the liver and that POSTN co-localized with α-SMA and collagen I in metastatic livers (Fig. 4i). These data suggest that overexpression of POSTN in the liver promotes the formation of a fibrotic microenvironment and the metastatic growth of CRC cells in mouse livers.

POSTN promotes the expression of TGF-β1 in colorectal tumour cells by activating the integrin/FAK/ERK/STAT3 pathway

Having demonstrated that HSC-derived POSTN promotes liver metastatic colonization of CRC tumour cells, we further determined the cytokines from colorectal tumour cells that could be induced by HSC-derived POSTN. Previous studies have shown that high levels of TGF-β1 in the serum of patients with CRC are associated with poor outcomes, and elevation of TGF-β levels in colorectal tumour cells enhances the efficiency of liver colonization [5, 23]. Interestingly, our data revealed that POSTN deficiency or decreased, whereas POSTN overexpression increased, the expression of *Tgfb1* in colorectal tumours (Figs. 1c, 2g, 3g, 4g). Moreover, current reports have demonstrated that POSTN can induce TGF-β expression in inflammatory microenvironment [11, 24]; however, the exact underlying regulatory mechanism remains unclear. To determine whether POSTN induces TGF-β/Smad signal transduction in colorectal tumour cells, we measured the mRNA level of *Tgfb1* in colorectal tumour cells upon POSTN stimulation. We found that treatment with mouse recombinant POSTN (rmPOSTN) upregulated the mRNA level of *Tgfb1* in mouse CMT93 colorectal tumour cells (Fig. 5a). We further treated mouse (CMT93) and human (SW620) colorectal tumour cells with mouse and human recombinant POSTN protein, respectively, and found that the phosphorylation of FAK, ERK, and STAT3 was increased by POSTN stimulation (Fig. 5b, c). The increase of FAK, ERK, and STAT3 phosphorylation induced by POSTN treatment was impaired in CMT93 and SW620 cells after pre-incubation with antibodies against the POSTN receptors αvβ3 or αvβ5 integrins (Fig. 5b, c), or with the p-FAK inhibitor PF573228 (Fig. 5d, e). Moreover, the upregulation of *Tgfb1* mRNA levels in CMT93 and SW620 cells

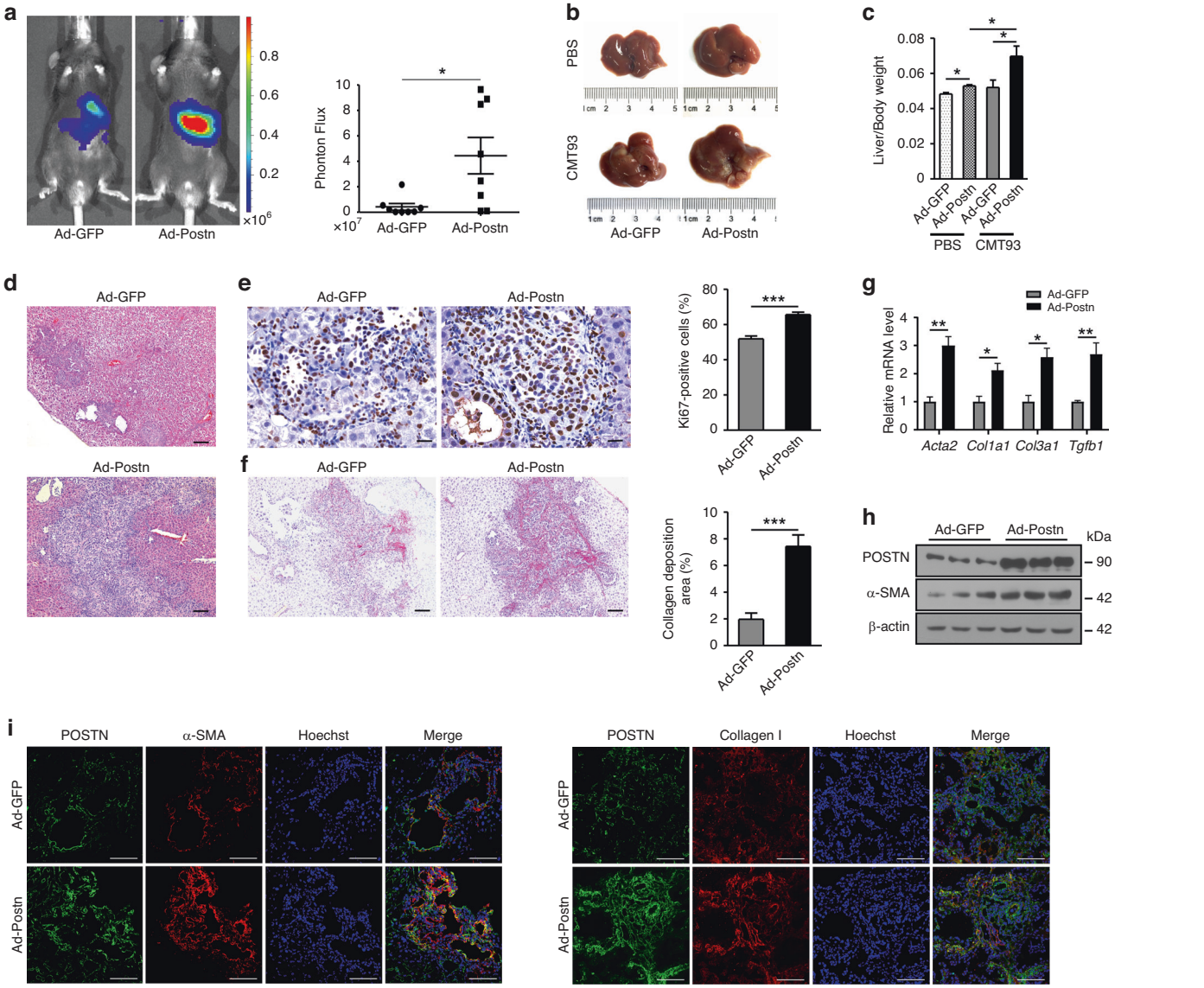

Fig. 4 Overexpression of POSTN in the livers promotes the fibrotic metastatic microenvironment formation and metastatic growth of colorectal tumour cells. a Bioluminescent imaging and quantification of metastatic lesions in mice 14 days after intrasplenic implantation of CMT93-Luc cells. These mice were infected with adenovirus containing GFP (Ad-GFP) or *Postn* (Ad-Postn) by tail vein injection 2 days after cell injection ($n = 8$ per group). Representative liver images (**b**) and liver:body weight ratio (**c**) of mice with indicated treatment. **d** H&E staining of metastatic liver sections of mice 14 days after cell injection. Scare bars, 100 μm. **e** Representative immunohistochemical staining images and the quantification of Ki67-positive tumour cells in metastatic livers of mice. Scare bars, 100 μm. **f** Sirius Red staining and the quantification of collagen deposition. Scare bars, 50 μm. **g** qRT-PCR analysis for mRNA levels of the indicated fibrotic genes. Western blot analysis of POSTN and α-SMA (**h**) and immunofluorescent co-staining for POSTN and α-SMA/collagen I (**i**) in metastatic livers. Scare bars, 100 μm. *, $p < 0.05$; **, $p < 0.01$; ***, $p < 0.001$.

induced by POSTN treatment was impaired by pre-incubation with PF573228 (Fig. 5d, e, lower panels). Furthermore, inhibition of ERK signalling with PD98059 treatment decreased the level of phosphorylated STAT3 and the mRNA level of *Tgfb1* but had no effect on the level of phosphorylated FAK (Fig. 5f, g). The ELISA and immunofluorescence results showed that the upregulation of TGF-β1 levels in CMT93 and SW620 cells induced by POSTN treatment was impaired by pre-incubation with PF573228 or PD98059 (Supplementary Fig. S3 and S4). STAT3 was shown to directly bind to the *Tgfb1* promoter to induce its expression [25]. Indeed, the mRNA level of *Tgfb1* was significantly decreased by treatment with Stattic, a STAT3 inhibitor (Fig. 5h, i). Moreover, knockdown of STAT3 using short interfering RNAs (siRNAs) impaired rmPOSTN-induced *Tgfb1* mRNA expression in colorectal tumour cells (Fig. 5j, k). We also found that the levels of phosphorylated FAK, ERK, and STAT3 in the metastatic livers of *Postn*-knockout mice were lower, whereas Ad-Postn mice were higher, than those in control mice (Supplementary Fig. S5A, B). Moreover, the colorectal tumour cells isolated from metastatic lesions expressed high levels of TGF-β1, but the tumour cells isolated from metastatic lesions of *Postn*-knockout mice showed decreased levels of *Tgfb1* compared to those from wild-type mice (Supplementary Fig. S5C). Immunohistochemical staining showed that the accumulation of phosphorylated STAT3 was significantly decreased in the metastatic livers of *Postn*-knockout mice (Supplementary Fig. S6A). In contrast, Ad-Postn overexpression increased the levels of phosphorylated STAT3 in the metastatic livers of mice injected with CRC cells (Supplementary Fig. S6B). Moreover, we found higher levels of phosphorylated STAT3 in metastatic liver tumours of CRC patients compared to adjacent

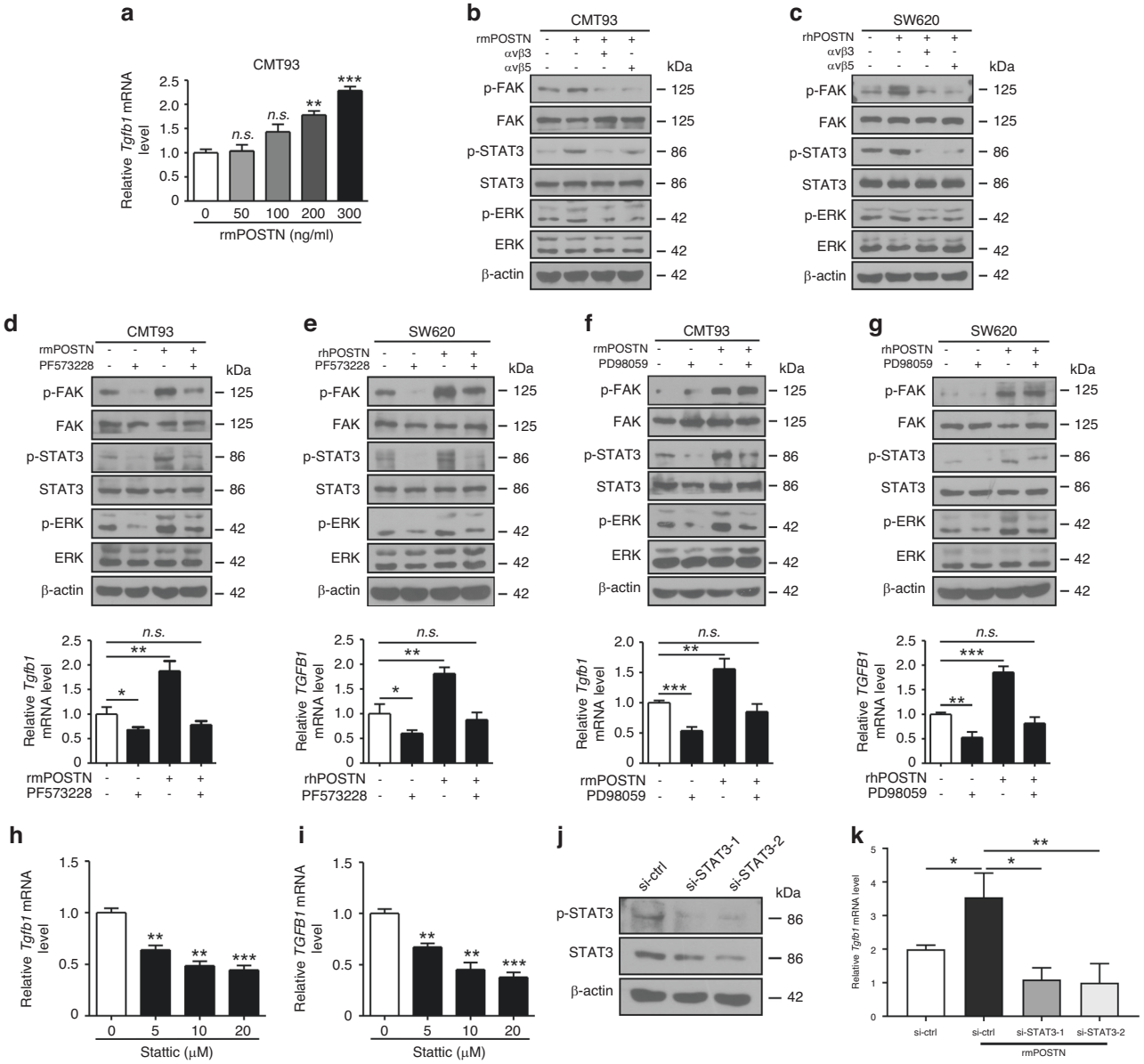

Fig. 5 POSTN promotes the expression of TGF-β1 in CRC cells by activating the integrin/FAK/ERK/STAT3 pathway. a qRT-PCR analysis of the mRNA level of *Tgfb1* in CMT93 cells treated with different concentrations of rmPOSTN. Western blot analysis of the levels of p-FAK, FAK, p-ERK, ERK, p-STAT3 and STAT3 in CMT93 (**b**) and SW620 (**c**) cells pre-incubated with antibodies against αvβ3 or αvβ5 integrins and rmPOSTN or rhPOSTN. Western blot analysis of the levels of p-FAK, FAK, p-ERK, ERK, p-STAT3 and STAT3 (upper panels) and qRT-PCR analysis of *Tgfb1* mRNA (lower panels) in CMT93 (**d**) or SW620 (**e**) cells pre-incubated with or without the p-FAK inhibitor PF573228 and treated with rmPOSTN or rhPOSTN. Western blot analysis of the levels of p-FAK, FAK, p-ERK, ERK, p-STAT3 and STAT3 (upper panels) and qRT-PCR analysis of *Tgfb1* mRNA (lower panels) in CMT93 (**f**) or SW620 (**g**) cells pre-incubated with or without the p-ERK inhibitor PD98059 and treated with rmPOSTN or rhPOSTN. qRT-PCR analysis of the mRNA level of *Tgfb1* in CMT93 (**h**) and SW620 (**i**) cells treated with different dosages of p-STAT3 inhibitor Stattic. **j** Western blot analysis of the levels of p-STAT3 and STAT3 in CMT93 cells transfected with si-Ctrl or siRNAs to knockdown STAT3. **k** qRT-PCR assay of the mRNA levels of *Tgfb1* in rmPOSTN-treated CMT93 cells transfected with indicated siRNAs ($n = 3$ per group). *, $p < 0.05$; **, $p < 0.01$; ***, $p < 0.001$; n.s., not significant.

tissues (Supplementary Fig. S6C). These data suggest that POSTN can induce TGF-β expression in colorectal tumour cells by activating the integrin/FAK/ERK/STAT3 signalling pathway.

TGF-β promotes the expression of POSTN in HSCs via Smad pathway

Having demonstrated that HSC-derived POSTN can induce the expression of TGF-β1 in colorectal tumour cells, we further determined whether tumour cell-derived TGF-β1 can promote the expression of POSTN in activated HSCs in a positive feedback manner. Previous studies have demonstrated that TGF-β induces POSTN expression in stromal cells [14, 26]; however, the underlying mechanisms remain largely unknown. We stimulated human HSCs with recombinant human TGF-β1 (rhTGF-β1) and found that rhTGF-β1 treatment increased *POSTN* mRNA expression in human HSC LX-2 cells in a dose-dependent manner (Fig. 6a). Moreover, knockdown of Smad3 using short interfering RNAs (siRNAs) impaired rhTGF-β1-induced POSTN expression in LX-2 cells (Fig. 6b, c). We also found that the expression of POSTN and phosphorylated Smad3 was enhanced in LX-2 cells when indirectly co-cultured with SW620 colorectal tumour cells in vitro (Fig. 6d, e). To further determine whether POSTN is a direct target

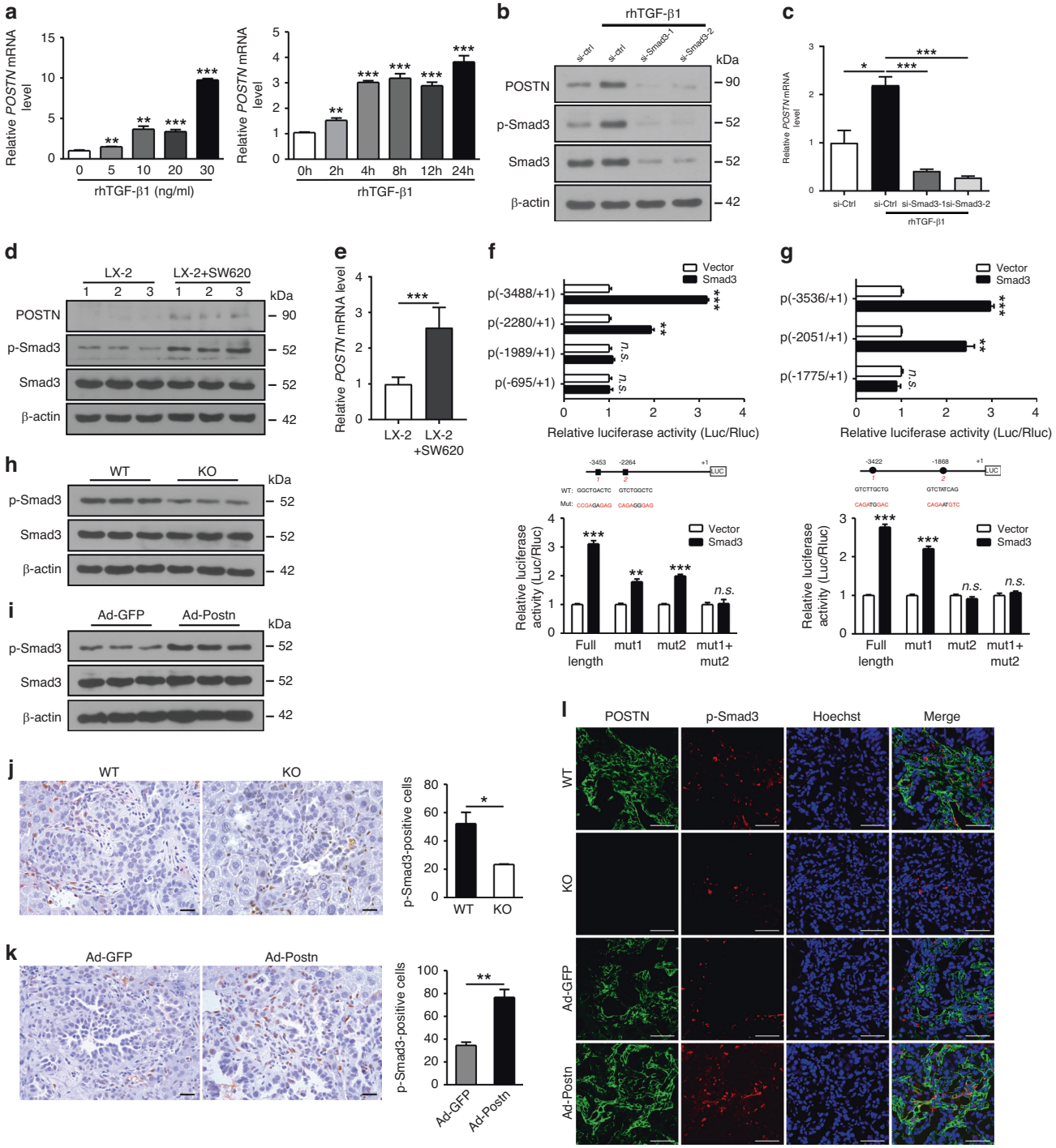

Fig. 6 TGF-β promotes POSTN expression in HSCs via the Smad signalling pathway. a qRT-PCR analysis of *POSTN* mRNA levels in LX-2 cells treated with different concentrations of rhTGF-β1 and 10 ng/ml rhTGF-β1 at different time points. Western blot analysis of POSTN, Smad3, and p-Smad3 levels (**b**) and qRT-PCR analysis of *POSTN* mRNA levels (**c**) in LX-2 cells with siRNA-transfected and stimulated with rhTGF-β1. **d** Western blot analysis of POSTN, Smad3 and p-Smad3 in LX-2 cells cultured alone or indirectly co-cultured with human SW620 cells. **e** qRT-PCR analysis of *POSTN* mRNA levels in LX-2 cells cultured alone or indirectly co-cultured with human SW620 cells. The localization of mouse (**f**) and human (**g**) Smad3 responsive elements in the *POSTN* promoter (upper panels) and the effects of point mutations to identify Smad3-responsive regions (lower panels) using a dual-luciferase reporter system. Luciferase activities were normalized by firefly luciferase and Renilla luciferase ratio and expressed as fold induction relative to control cultures, defined as 1. **h** Western blot analysis of the levels of phosphorylated Smad3 in the metastatic livers of wild-type or *Postn*-knockout mice. **i** Western blot analysis of the level of phosphorylated Smad3 in the metastatic livers of mice infected with Ad-GFP or Ad-Postn via tail vein injection. **j** Immunohistochemical staining for p-Smad3 and quantitative analysis of phosphorylated Smad3-positive cells in the metastatic livers of wild-type and *Postn*-knockout mice. Scare bars, 50 μm. **k** Immunohistochemical staining for phosphorylated Smad3 and quantitative analysis of phosphorylated Smad3-positive cells in metastatic livers of mice infected with Ad-GFP or Ad-Postn via tail vein injection. Scare bars, 50 μm. **l** Immunofluorescence co-staining for POSTN and p-Smad3 in metastatic livers of mice. Scare bars, 100 μm. *, $p < 0.05$; **, $p < 0.01$; ***, $p < 0.001$; n.s., not significant.

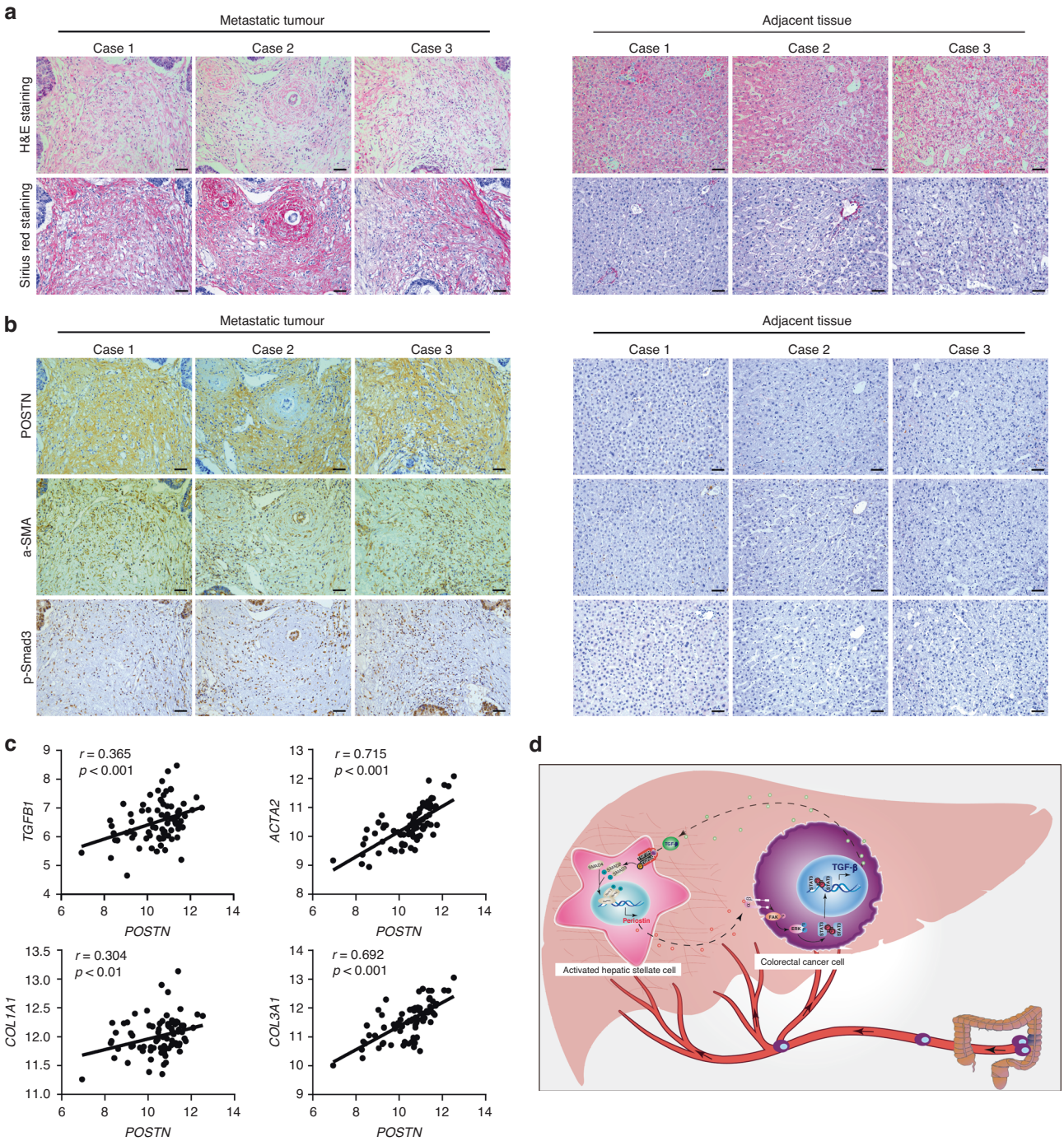

Fig. 7 POSTN level correlates with fibrotic features and TGF-β signalling in metastatic liver tissues of CRC patients. a H&E staining (upper panels) and Sirius Red staining (lower panels) of metastatic liver tissues and adjacent tissues of patients with CRC. Scare bars, 50 μm. **b** Immunohistochemical analysis of the expression of POSTN, α-SMA and phosphorylated Smad3 in metastatic liver tumours and adjacent tissues of CRC patients. Scare bars, 50 μm. **c** Correlation analysis of *POSTN* mRNA with *TGFB1* and other fibrotic markers including *ACTA2*, *COL1A1* and *COL3A1* in metastatic liver tumours of CRC patients ($n = 79$) from R2 Database. Pearson correlation coefficient (r) and *P* value (*p*) are shown. **d** Schematic model of tumour-stroma crosstalk via HSC-derived POSTN and tumour cell-derived TGF-β in liver metastasis of CRC cells.

of TGF-β/Smad signalling, we investigated the transcriptional regulation of Smad3 on POSTN expression using a dual-luciferase reporter system. As shown in Figs. 6f, g, overexpression of Smad3 in 293 T cells resulted in enhanced luciferase activity, which was used to monitor the transcriptional activity of mouse or human *POSTN* promoters. We then performed a reporter assay using a series of truncated mutants to identify the minimal promoter required for *POSTN* transcription. We found two critical DNA regions for Smad3-induced transcriptional activity within mouse and human *POSTN* promoters (Fig. 6f, g). To further identify the core transcription region within the *POSTN* promoters, we generated mutant *POSTN* promoter constructs (Mut) containing mutations in the Smad-binding element domain by site-directed mutagenesis. We found that promoter activity induced by Smad3 was partially abolished upon mutation of the first or second site of the mouse *Postn* promoter, while the promoter activity was nearly

completely abolished upon mutation of the second site of the human *POSTN* promoter (Fig. 6f, g). To further determine whether TGF-β1 triggers POSTN expression through the downstream Smad-dependent pathway, we found that the levels of phosphorylated Smad3 were decreased in the metastatic liver extracts from *Postn*-knockout mice but increased in Ad-Postn mice, compared to their control (Fig. 6h, i). Immunohistochemical staining demonstrated that the accumulation of phosphorylated Smad3 was significantly decreased in the metastatic livers of *Postn*-knockout mice (Fig. 6j). In contrast, POSTN overexpression increased the levels of phosphorylated Smad3 in the metastatic livers of mice injected with CRC cells (Fig. 6k).

We also observed increased POSTN expression and p-Smad3 accumulation in activated HSCs in the metastatic livers of mice (Fig. 6l). These results indicate that TGF-β/Smad signalling can directly enhance the transcriptional activity of the *Postn* promoter, thereby potentiating the expression of POSTN in HSCs in metastatic livers.

POSTN level correlates with fibrotic features and TGF-β signalling in metastatic liver tissues of CRC patients

Next, we analyzed the correlation between POSTN expression, fibrotic features, and TGF-β signalling in the metastatic livers of patients with CRC. Sirius Red staining revealed increased collagen deposition in metastatic tumour tissues compared to adjacent tissues, indicating that a fibrotic microenvironment is also formed in the clinical metastatic liver samples (Fig. 7a). Moreover, immunohistochemical assays demonstrated that high levels of POSTN were deposited in the stromal areas of metastatic liver samples, in which α-SMA expression could also be detected, while the staining signals in adjacent tissues were negative (Fig. 7b). A large proportion of stromal cells with phosphorylated Smad3 was greatly increased in the fibrotic metastatic livers of patients with CRC (Fig. 7b). We also found that there was a positive correlation between *POSTN* levels and fibrotic markers, including *TGFB1*, *ACTA2*, *COL1A1* and *COL3A1* in CRC patients with liver metastases by analyzing microarray data from the R2 database (Fig. 7c). These results suggest that POSTN levels correlate with fibrotic features and TGF-β signalling in metastatic liver tissues of patients with CRC.

DISCUSSION

Metastatic outgrowth in the liver is a major cause of mortality in patients with CRC. The hepatic microenvironment can provide cues to drive cell adhesion, survival, and the outgrowth of metastatic CRC cells in the liver. Metastatic tumour cells interact with their neighbouring stromal cells to establish a supportive microenvironment in the metastatic liver [27]. Many studies have determined that activated HSCs are the main source of ECM, and the number of activated HSCs is significantly increased in the metastatic livers of CRC [28, 29]. Activated HSCs can create a tumour-supportive microenvironment that facilitates tumour metastasis [30, 31]. Previous studies have demonstrated that POSTN can induce a fibrotic microenvironment to support the growth of primary and metastatic pancreatic cancer [32, 33]. We also found that activated HSC-derived POSTN promoted the formation of a fibrotic microenvironment in the livers of mice with acute or chronic liver inflammation and in the liver tumours of mice treated with DEN [11, 22]. Here, we found that POSTN is mainly derived from activated HSCs and is largely distributed in the fibrotic microenvironment of metastatic liver. Knockout of *Postn* alleviates the formation of a fibrotic microenvironment and inhibits liver metastasis of colorectal tumour cells in mice, whereas overexpression of POSTN in the liver promotes fibrotic metastatic microenvironment formation and augments metastatic outgrowth of CRC cells in the liver. These data suggest that activated HSCs secrete POSTN to form a fibrotic microenvironment that supports the metastatic outgrowth of colorectal tumour cells in the liver.

As a matricellular protein, POSTN plays a critical role in mediating crosstalk between tumour cells and stromal cells in tumour microenvironments during tumourigenesis and metastasis [14, 17–19, 22]. In lung metastasis of breast cancer, breast cancer stem cell (CSC)-derived TGF-β can induce POSTN expression in cancer-associated fibroblasts (CAFs), whereas CAF-derived POSTN can augment Wnt signalling to promote CSC self-renewal and metastatic colonization in the lungs [14]. In B-cell acute lymphoblastic leukaemia (B-ALL), bone marrow-derived mesenchymal stromal cells (BM-MSCs) express high levels of POSTN and promote leukaemia cells secretion of CCL2 via integrin/ILK/NF-κB signalling, whereas leukaemia cell-derived CCL2 increases POSTN expression in BM-MSCs through the CCR2/STAT3 pathway [17]. In colorectal tumours, we found that *Postn* knockout inhibits tumourigenesis in AOM/DSS-treated mice and $APC^{min/+}$ mice. Colorectal tumour cell-derived IL-6 can induce the expression of POSTN in fibroblasts and fibroblast-derived POSTN stimulates the expression of IL-6 in tumour cells, indicating that fibroblast-derived POSTN cooperates with tumour cell-derived IL-6 to promote the development of colorectal tumours [18]. Recently, we further demonstrated that CAF-derived POSTN increases $PD\text{-}1^{+}$ TAM infiltration and immune evasion of tumour cells, and the combined blockage of POSTN and PD-1 significantly inhibits tumour progression in mouse CRC [19]. Previously, we found that ectopic overexpression of POSTN in colon cancer cells promotes the metastatic growth of colon cancer cells in the livers of mice [20]. It is well known that CRC cells secrete multiple growth factors, including TGF-β, to activate HSCs, and that TGF-β promotes liver metastasis of CRC [5, 34, 35]. However, the mechanism by which POSTN regulates TGF-β expression and how TGF-β induces POSTN expression in tumourigenesis and metastasis of CRC remain largely unknown. Here, we found that colorectal tumour cells produce high levels of TGF-β to promote the activation of HSCs into α-SMA-positive myofibroblasts, which supports liver metastasis of tumour cells by secreting large amounts of POSTN to provide a supportive fibrotic microenvironment. We also found that activated HSC-derived POSTN stimulates TGF-β expression in colorectal tumour cells via the integrin/FAK/ERK/STAT3 pathway. These data suggest that POSTN and TGF-β play a critical role in mediating the crosstalk between tumour cells and HSCs in the hepatic fibrotic microenvironment during the liver metastasis of CRC cells.

In conclusion, metastatic colorectal tumour cells educate and activate HSCs to produce excessive amounts of POSTN and other ECM proteins to form a fibrotic metastatic microenvironment via the TGF-β/Smad pathway. In turn, activated HSC-derived POSTN increases the expression of TGF-β in CRC cells by activating the integrin/FAK/ERK/STAT3 signalling pathway. Thus, colorectal tumour cell-derived TGF-β and activated HSC-derived POSTN cooperatively promote the formation of a fibrotic metastatic microenvironment and the metastatic outgrowth of colorectal tumour cells in the liver through tumour-stroma crosstalk (Fig. 7d). The discovery of POSTN–TGF-β feedforward loop between tumour cells and activated HSCs might provide a potential target for destroying tumour-stroma crosstalk to inhibit the formation of a hepatic fibrotic microenvironment and decrease liver metastasis of colorectal tumour cells.

DATA AVAILABILITY

All data are present in the manuscript and the Supplementary Materials. Additional data related to this paper may be requested from the corresponding author.

REFERENCES

1. Sung H, Ferlay J, Siegel RL, Laversanne M, Soerjomataram I, Jemal A, et al. Global Cancer Statistics 2020: GLOBOCAN estimates of incidence and mortality worldwide for 36 cancers in 185 countries. CA Cancer J Clin. 2021;71:209–49.
2. Wu Y, Yang S, Ma J, Chen Z, Song G, Rao D, et al. Spatiotemporal immune landscape of colorectal cancer liver metastasis at single-cell level. Cancer Discov. 2022;12:134–53.

3. Bertocchi A, Carloni S, Ravenda PS, Bertalot G, Spadoni I, Lo Cascio A, et al. Gut vascular barrier impairment leads to intestinal bacteria dissemination and colorectal cancer metastasis to liver. Cancer Cell. 2021;39:708–24.e11.
4. Zhou H, Liu Z, Wang Y, Wen X, Amador EH, Yuan L, et al. Colorectal liver metastasis: molecular mechanism and interventional therapy. Signal Transduct Target Ther. 2022;7:70.
5. Calon A, Espinet E, Palomo-Ponce S, Tauriello DV, Iglesias M, Céspedes MV, et al. Dependency of colorectal cancer on a TGF-β-driven program in stromal cells for metastasis initiation. Cancer Cell. 2012;22:571–84.
6. Ouahoud S, Voorneveld PW, van der Burg LRA, de Jonge-Muller ESM, Schoonderwoerd MJA, Paauwe M, et al. Bidirectional tumor/stroma crosstalk promotes metastasis in mesenchymal colorectal cancer. Oncogene. 2020;39:2453–66.
7. Zhao S, Mi Y, Zheng B, Wei P, Gu Y, Zhang Z, et al. Highly-metastatic colorectal cancer cell released miR-181a-5p-rich extracellular vesicles promote liver metastasis by activating hepatic stellate cells and remodelling the tumour microenvironment. J Extracell Vesicles. 2022;11:e12186.
8. Bissell MJ, Radisky D. Putting tumours in context. Nat Rev Cancer. 2001;1:46–54.
9. Kai F, Drain AP, Weaver VM. The extracellular matrix modulates the metastatic journey. Dev Cell. 2019;49:332–46.
10. Shimazaki M, Nakamura K, Kii I, Kashima T, Amizuka N, Li M, et al. Periostin is essential for cardiac healing after acute myocardial infarction. J Exp Med. 2008;205:295–303.
11. Huang Y, Liu W, Xiao H, Maitikabili A, Lin Q, Wu T, et al. Matricellular protein periostin contributes to hepatic inflammation and fibrosis. Am J Pathol. 2015;185:786–97.
12. Ono J, Takai M, Kamei A, Azuma Y, Izuhara K. Pathological roles and clinical usefulness of periostin in type 2 inflammation and pulmonary fibrosis. Biomolecules. 2021;11:1084.
13. Nanri Y, Nunomura S, Honda Y, Takedomi H, Yamaguchi Y, Izuhara K A positive loop formed by SOX11 and periostin upregulates TGF-β signals leading to skin fibrosis. J Invest Dermatol. (2022):S0022-202X(22)02902–5.
14. Malanchi I, Santamaria-Martínez A, Susanto E, Peng H, Lehr HA, Delaloye JF, et al. Interactions between cancer stem cells and their niche govern metastatic colonization. Nature. 2012;481:85–9.
15. Wang Z, Ouyang G. Periostin: a bridge between cancer stem cells and their metastatic niche. Cell Stem Cell. 2012;10:111–2.
16. Conway SJ, Izuhara K, Kudo Y, Litvin J, Markwald R, Ouyang G, et al. The role of periostin in tissue remodeling across health and disease. Cell Mol Life Sci. 2014;71:1279–88.
17. Ma Z, Zhao X, Deng M, Huang Z, Wang J, Wu Y, et al. Bone marrow mesenchymal stromal cell-derived periostin promotes B-ALL progression by modulating CCL2 in leukemia cells. Cell Rep. 2019;26:1533–43.e4.
18. Ma H, Wang J, Zhao X, Wu T, Huang Z, Chen D, et al. Periostin promotes colorectal tumorigenesis through integrin-FAK-Src pathway-mediated YAP/TAZ activation. Cell Rep. 2020;30:793–806.e6.
19. Wei T, Wang K, Liu S, Fang Y, Hong Z, Liu Y, et al. Periostin deficiency reduces PD-1+ tumor-associated macrophage infiltration and enhances anti-PD-1 efficacy in colorectal cancer. Cell Rep. 2023;42:112090.
20. Bao S, Ouyang G, Bai X, Huang Z, Ma C, Liu M, et al. Periostin potently promotes metastatic growth of colon cancer by augmenting cell survival via the Akt/PKB pathway. Cancer Cell. 2004;5:329–39.
21. Lu Y, Liu X, Jiao Y, Xiong X, Wang E, Wang X, et al. Periostin promotes liver steatosis and hypertriglyceridemia through downregulation of PPARα. J Clin Invest. 2014;124:3501–13.
22. Xiao H, Zhang Y, Li Z, Liu B, Cui D, Liu F, et al. Periostin deficiency reduces diethylnitrosamine-induced liver cancer in mice by decreasing hepatic stellate cell activation and cancer cell proliferation. J Pathol. 2021;255:212–23.
23. Tsushima H, Ito N, Tamura S, Matsuda Y, Inada M, Yabuuchi I, et al. Circulating transforming growth factor beta 1 as a predictor of liver metastasis after resection in colorectal cancer. Clin Cancer Res. 2001;7:1258–62.
24. Lorts A, Schwanekamp JA, Baudino TA, McNally EM, Molkentin JD. Deletion of periostin reduces muscular dystrophy and fibrosis in mice by modulating the transforming growth factor-β pathway. Proc Natl Acad Sci USA. 2012;109:10978–83.
25. Kinjyo I, Inoue H, Hamano S, Fukuyama S, Yoshimura T, Koga K, et al. Loss of SOCS3 in T helper cells resulted in reduced immune responses and hyperproduction of interleukin 10 and transforming growth factor-β1. J Exp Med. 2006;203:1021–31.
26. Chen G, Nakamura I, Dhanasekaran R, Iguchi E, Tolosa EJ, Romecin PA, et al. Transcriptional induction of periostin by a sulfatase 2-TGFβ1-SMAD signaling axis mediates tumor angiogenesis in hepatocellular carcinoma. Cancer Res. 2017;77:632–45.
27. Tan HX, Gong WZ, Zhou K, Xiao ZG, Hou FT, Huang T, et al. CXCR4/TGF-β1 mediated hepatic stellate cells differentiation into carcinoma-associated fibroblasts and promoted liver metastasis of colon cancer. Cancer Biol Ther. 2020;21:258–68.
28. Badiola I, Olaso E, Crende O, Friedman SL, Vidal-Vanaclocha F. Discoidin domain receptor 2 deficiency predisposes hepatic tissue to colon carcinoma metastasis. Gut. 2012;61:1465–72.
29. Reszegi A, Horváth Z, Karászi K, Regős E, Postniková V, Tátrai P, et al. The protective role of decorin in hepatic metastasis of colorectal carcinoma. Biomolecules. 2020;10:1199.
30. Coulouarn C. Modulating the activation of hepatic stellate cells: a cunning way for metastatic cells to create a permissive soil for seeding in the liver? Hepatology. 2015;61:37–40.
31. Tsilimigras DI, Brodt P, Clavien PA, Muschel RJ, D'Angelica MI, Endo I, et al. Liver metastases. Nat Rev Dis Primers. 2021;7:27.
32. Erkan M, Kleeff J, Gorbachevski A, Reiser C, Mitkus T, Esposito I, et al. Periostin creates a tumor-supportive microenvironment in the pancreas by sustaining fibrogenic stellate cell activity. Gastroenterology. 2007;132:1447–64.
33. Nielsen SR, Quaranta V, Linford A, Emeagi P, Rainer C, Santos A, et al. Macrophage-secreted granulin supports pancreatic cancer metastasis by inducing liver fibrosis. Nat Cell Biol. 2016;18:549–60.
34. Wang Y, Tu K, Liu D, Guo L, Chen Y, Li Q, et al. p300 acetyltransferase is a cytoplasm-to-nucleus shuttle for SMAD2/3 and TAZ nuclear transport in transforming growth factor β-stimulated hepatic stellate cells. Hepatology. 2019;70:1409–23.
35. Qi M, Fan S, Huang M, Pan J, Li Y, Miao Q, et al. Targeting FAPα-expressing hepatic stellate cells overcomes resistance to antiangiogenics in colorectal cancer liver metastasis models. J Clin Invest. 2022;132:e157399.

ACKNOWLEDGEMENTS

We are deeply grateful to Prof. Xiaoying Li for providing recombinant adenoviruses and Dr. Fan Liu and Dr. Dan Cui for their valuable support.

AUTHOR CONTRIBUTIONS

BL, TW, BLin, XL and CF acquired experimental data. BL, TW, BLin, GS, CF and GO were involved in manuscript writing. BL, TW, BLin, YL, GS, CF and GO analyzed the data. TW, GS and GO obtained funding. All authors read and approved the final manuscript.

FUNDING

This work was supported by grants from the National Natural Science Foundation of China (81772616, 81470793, 81972748, 82172932, and 82273416) and the Natural Science Foundation of Fujian Province of China (2019J02002).

COMPETING INTERESTS

The authors declare no competing interests.

ETHICS APPROVAL AND CONSENT TO PARTICIPATE

Human clinical samples were collected with informed consent from the patients. The collection and study of human clinical samples were performed in accordance with the approved guidelines of the Ethics and Scientific Committees of Xiamen Hospital of Traditional Chinese Medicine.

ADDITIONAL INFORMATION

Supplementary information The online version contains supplementary material available at https://doi.org/10.1038/s41416-023-02516-3.

Correspondence and requests for materials should be addressed to Gang Song, Chuannan Fan or Gaoliang Ouyang.